jp509513s-1 page numbers

DATASET · MARCH 2015

READS
22

2 AUTHORS:

Antti Lignell
California Institute of Technology
44 PUBLICATIONS **846** CITATIONS
SEE PROFILE

Murthy S Gudipati
California Institute of Technology
119 PUBLICATIONS **928** CITATIONS
SEE PROFILE

THE JOURNAL OF PHYSICAL CHEMISTRY A

Article

pubs.acs.org/JPCA

Mixing of the Immiscible: Hydrocarbons in Water-Ice near the Ice Crystallization Temperature

Antti Lignell[‡] and Murthy S. Gudipati*[,§]

Ice Spectroscopy Lab, Science Division, Jet Propulsion Laboratory, California Institute of Technology, 4800 Oak Grove Drive, Pasadena, California 91109, United States

ABSTRACT: Structural changes in hydrocarbon-doped water-ice during amorphous to crystalline phase conversion are investigated using polycyclic aromatic hydrocarbons (PAHs) as probes. We show that aggregation of impurity molecules occurs due to the amorphous−crystalline transition in ice, especially when they are hydrophobic molecules such as PAHs. Using ultraviolet−visible (UV−vis), Fourier-transform Infrared (FTIR), and laser-induced-fluorescence (LIF) spectroscopic techniques, we show that, although ice infrared absorption features change from a broad structureless band corresponding to amorphous ice to a sharp structured crystalline ice bands, simultaneously, sharper isolated PAH UV absorption features measured in the amorphous ice host turn broad upon ice crystallization. A simultaneous decrease in the monomer fluorescence and increase in the excimer emission band is observed, a clear indication for the formation of PAH molecular aggregates when amorphous ice is converted to crystalline ice at higher temperatures. Similar to the irreversible amorphous−crystalline phase transitions, the UV, fluorescence, and excimer emissions indicate that PAHs undergo irreversible aggregation. Our studies suggest that organic impurities exist as aggregates rather than monomers trapped in crystalline water-ice when cycled through temperatures that convert amorphous ice to crystalline ice, rendering a better insight into phenomena such as the formation of cometary crust. This aggregate formation also may significantly change the secondary reaction pathways and rates in impurity-doped ices in the lab, on Earth, in the solar system, and in the interstellar medium.

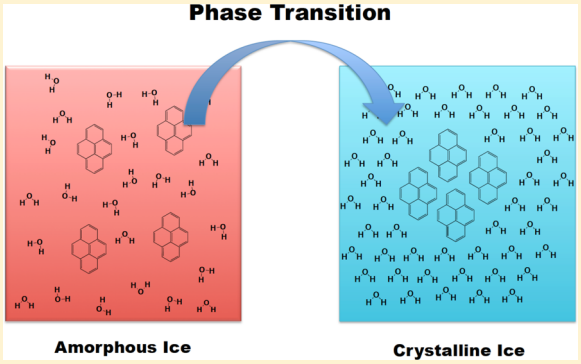

INTRODUCTION

Water-ice is found in a wide variety of conditions in Space and close to us on Earth. Under interstellar conditions amorphous ice dominates the water-rich grains containing a wide variety of organic impurities.[1,2] On the other hand, only crystalline ice has been observed on the icy surfaces so far investigated in our own solar system, from Earth's ices at 1 AU to far away Trans-Neptunian-Objects (TNOs) and Kuiper-Belt-Objects (KBOs) at tens of AU distance, where the temperatures are as low as 30−50 K.[3−5] The dominance of crystalline icy surfaces in the solar system, where amorphous ices are expected to dominate, is still an unresolved puzzle and puts a bottleneck in our understanding of the evolution of interstellar ice grains into solar system icy bodies. In particular, comets that originate from KBOs and the Oort Cloud are supposed to retain the primordial composition of interstellar ice grains in their nucleus. It is unclear whether a comet's interior is composed of amorphous or crystalline ices. Amorphous ice is known to accommodate a large fraction of impurities.[6] Earlier observations of sudden and explosive decomposition of comets have been rationalized on potential exothermic crystallization of amorphous ices in a comet's nucleus, which is still under debate.[7−10] One of the working postulates of the origin of life on Earth is through comet and asteroid impacts on early Earth that could have brought the needed organics and water facilitating the origin of life soon after the lunar cataclysm, also known as the late heavy bombardment (LHB).[11−16] Thus, crystallization of amorphous ices has important implications to our understanding of chemistry and physics of interstellar and solar system ices. Ice found on the Moon's permanently shadowed cold regions, where temperatures could reach as low as 30 K, could potentially stay amorphous if condensed from the gas-phase water. However, no information is yet available on the phase behavior of lunar ice.

On Earth ice plays an equally important role in keeping the delicate thermal balance through polar ice caps, glaciers, and ice packs at high-altitude mountains. Atmospheric ices such as the cirrus clouds, polar stratospheric clouds (PSCs), and polar mesospheric clouds (PMCs) also play an important role in global and local atmospheres. Anthropogenic or natural contaminants reaching into these regions could cause chemical reactions that are otherwise inaccessible in pure ices. It is also important to understand how crystalline ices retain organic impurities under these conditions though amorphous ices are not expected to be present under these temperatures. Phase separation of ice and impurities when liquid water freezes is

Special Issue: Markku Räsänen Festschrift

Received: September 19, 2014
Revised: October 10, 2014
Published: October 10, 2014

well-known when oceans in the Polar Regions freeze, resulting in expulsion of salts and other impurities from water, resulting in purer water-ice.[17] Such a process of freeze-driven purification of salt water is also considered in desalination of ocean water.[18−20]

Aggregation of guest atoms and molecules in noble-gas matrixes due to increasing guest-to-host ratio,[21] through annealing[22] or through photomobility,[23,24] is a well-known phenomenon. Thermal annealing or photoinduced mobility gives energy to an atom/molecule to overcome the energy barrier between the matrix sites inducing diffusion of these species in the lattice. This diffusion eventually leads to multimer and aggregate formation. With increasing guest concentration, the average separation between the guest species shortens, leading to an increase in the probability of the formation of aggregates in the host matrix. The mechanism of the formation of aggregates in this work is different from the "traditional" thermally induced aggregate formation because in this case we exclusively link the clusterization into the phase transition of a media. To our best knowledge, this is the first time aggregate formation of a large hydrocarbon molecule is linked to the phase transition between amorphous and crystalline water-ice. Its exact mechanism is still unclear and exceeds the scope of this article. What is clear is that when the amorphous form is converted into crystalline form this change brings a less order and more porosity to more order and less porosity (disorder-to-order transition) matrix, making little or no room for guest molecules to be accommodated. It is likely that as the crystallization begins, these molecules are expelled from the crystal lattice resulting in the formation aggregates that most likely are now trapped between crystalline ice grain boundaries.

EXPERIMENTAL SECTION

All the experiments have been carried out at the *Ice Spectroscopy Lab (ISL)* at the Jet Propulsion Laboratory (JPL). Details of the cryogenic system used as well as the infrared and UV spectroscopic systems are given in a recent publication.[25] Briefly, a closed-cycle helium cryostat (APD) is mounted in a vacuum chamber having 8 ports (Kimball Physics 6″ Octagon). All the spectra were measured in transmission mode. Infrared (IR), ultraviolet (UV), and laser-induced-fluorescence (LIF) spectra were measured on the same sample simultaneously or subsequent to each other without changing the sample position. FTIR spectra were measured using a Thermo-Nicolet 6700 spectrometer with an MCT-B detector; UV spectra were measured using a deuterium-halogen dual source coupled with fiber optics collimated to pass through the sample and collected into another fiber optics cable that fed into Ocean Optics HR4000 or USB4000 spectrometers. LIF spectra were measured using a tunable optical parametric oscillator (OPO) laser source with UV-doubling option covering the 210 to 750 nm (OPOTEK Vibrant UV) spectral range. The pulse energy was ∼1 mJ/cm^2 and a repetition rate of 20 Hz was used. Fluorescence was collected through the same optical fiber and spectrometer that were used for UV absorption spectroscopy. A sketch of the experimental setup is shown in Figure 1.

Water vapor under high vacuum was passed over temperature-controlled (∼45 °C) pyrene crystals confined using Teflon-wool on both sides in a 0.25 in. outer diameter stainless steel deposition line. This procedure ensures that water vapor flows over the pyrene crystals and carries with it sublimed pyrene molecules. The typical pressure was 10^{-6} mbar during ice deposition and 10^{-9} mbar after deposition. Ice was

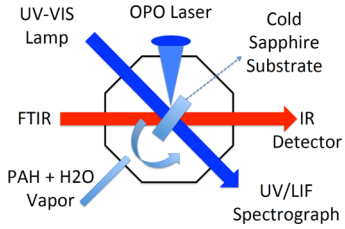

Figure 1. Simultaneous UV−vis, FTIR, and LIF spectroscopic studies on cryogenic ices. The sapphire substrate on which ice films were grown is mounted on the tip of a cryohead that can be rotated.

deposited for ∼30 min and ice film thickness was monitored using HeNe (632.8 nm) laser interferences, the typical ice thickness being ∼250−500 nm. On the basis of the ice thickness and UV band strengths of pyrene, a dilution factor of ∼1:500 is estimated for pyrene:water in the ice films. All the ice depositions were conducted at 30 K. For ice deposition the sapphire window (mounted at the tip of the cryostat) was rotated perpendicular to the deposition capillary (Figure 1). UV−vis and FTIR spectra measured before ice deposition at 30 K were used as reference spectra for the rest of the measurements. Subsequent to the deposition of ice at 30 K, which is clearly identified as amorphous ice on the basis of the IR spectra, ice films were warmed to 135 K and above, resulting in crystalline ices. At each temperature FTIR, UV−vis, and LIF spectra were measured after thermally equilibrating the ice at least for 30 min at the given temperature. The temperature ramp was typically 5 K min^{-1}. The IR, UV−vis, and LIF spectra are shown in Figures 2−4.

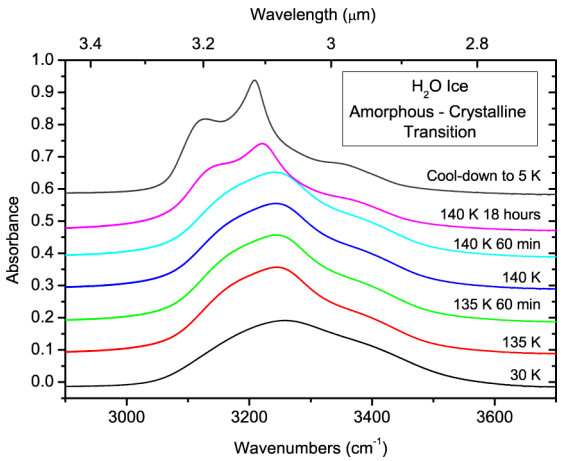

Figure 2. OH stretching region of the IR spectra of water-ice films doped with pyrene (PAH) molecules. Bottom: 30 K deposition resulting in amorphous ice. Top: after warming the ice to 140 K for 19 h that resulted in crystallization and then cooling the ice back to 5 K. Intermediate stages are captured in the spectra taken at 135 and 140 K at various stages.

Deposition rates, dilution, and sample thickness were controlled in such a way to obtain the best UV−vis and LIF spectra of the impurity PAH (pyrene) and the best IR spectra of water-ice. The concentration of pyrene and the thickness of the ice film were not high enough to observe pyrene IR spectral features, which typically would result in strong UV absorption (saturation) due to orders of magnitude differences in IR and UV absorption cross sections. Quantitative analysis of pyrene in

dx.doi.org/10.1021/jp509513s | J. Phys. Chem. A 2015, 119, 2607−2613

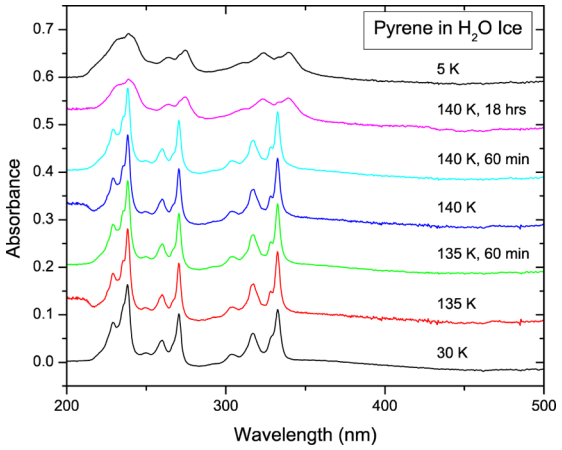

Figure 3. UV absorption spectra of water-ice films doped with pyrene (PAH) molecules. Spectra were taken at the same conditions as the IR spectra of water-ice shown in Figure 2. The majority of the pyrene molecules are isolated in their position until a long-period (18 h) warm-up was carried out at 140 K, resulting in aggregation of pyrene molecules in crystalline ice, which persists even after cooling back to 5 K.

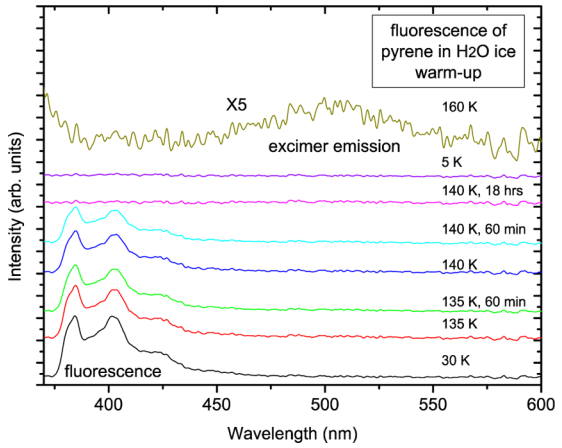

Figure 4. Laser-induced fluorescence (LIF) spectra of water-ice films doped with pyrene (PAH) molecules. Spectra were taken at same conditions as the IR and UV spectra shown in Figures 2 and 3. Fluorescence persists until a short warm-up at 140 K but completely disappears during the overnight warm-up at 140 K and cool-down to 5 K, in agreement with the formation of pyrene clusters seen in the UV spectra. Weak excimer emission is observed during subsequent warm-up to 165 K.

D_2O and H_2O ices has recently been published for further reading.[26]

RESULTS AND DISCUSSION

Vapor deposition of water at temperatures below 100 K results in the formation of amorphous ice, which is characterized by its broad and structureless absorption between 3000 and 3600 cm^{-1} with the absorption maximum around 3250 cm^{-1} (Figure 2). Amorphous ice is a metastable form of water-ice and so far only found in interstellar medium[1,27] and in the laboratory.[28,29] Warm-up to ∼150 K results in irreversible phase-transition to crystalline ice. The kinetics of crystallization of amorphous ice have been well known in the literature.[29−31] There have been estimates for the phase transition dynamics from amorphous to crystallize ice as summarized in a recent review by Mastrapa et al.[29] According to these estimates water-ice should crystallize in ∼5 min at 140 K or with an uncertainty of two different methods used at a maximum of 50 min. However, our experiments shown in Figures 2−4 clearly indicate that it takes several hours for the crystallization to occur at 140 K, showing that, at these temperatures and in the laboratory time scale, crystallization of amorphous ices is a relatively slow process at that temperature. We clearly see infrared absorption features of crystalline water-ice, with well developed absorption bands at around 3100, 3190, and 3350 cm^{-1} upon keeping the ice at 140 K for several hours. These crystalline absorptions features are enhanced upon cooling to 5 K, in agreement with the earlier literature findings.[32]

We followed the crystallization of amorphous ice through the electronic absorption and fluorescence spectra of impurity pyrene molecules (Figures 3 and 4) gaining more insight into the crystallization process itself. Pyrene monomer molecules trapped in ice show sharp UV-absorption features, with little or no shifts in the absorption maxima compared to noble-gas matrix isolation spectra, in accordance with the previous observations.[33] However, prolonged warm-up at 140 K resulted in red-shifted and broadened absorption of pyrene clusters, very similar to solid pyrene film absorption.[34] LIF spectra were measured at excitation wavelengths corresponding to the absorption maximum of an isolated monomer at 332 nm. Pyrene fluorescence emission was observed in the amorphous ice phase, but the fluorescence disappeared when ice crystallized (corresponding to the broadened UV absorption spectra), indicating pyrene aggregation due to expulsion from crystalline ice and quenching of fluorescence at 140 K and during the subsequent cooling at 5 K. As shown in Figure 3, only when the substrate temperature is raised above 140 K and crystallization occurs do we observe the excimer emission of pyrene.[35] As discussed below, excimer emission is far weaker than the monomer fluorescence, consequently making excimer emission difficult to see in our thinner samples (∼300 nm) due to fewer emitters. Under prolonged deposition (6 times thicker ice), we do see clear excimer emission.

During aggregate formation three important spectroscopic changes occur in pyrene: (a) shifting of the monomer absorption maximum by almost 10 nm (332−342 nm), (b) decrease in the molar extinction coefficient by about 40% (35000−21000),[34] and (c) decrease in fluorescence quantum yields due to excimer formation.[36] All these aspects are observed in our studies. Unlike liquid solvents where aggregates can reorient to form excimers during the excited lifetime of one of the excited molecules, in crystalline ice surroundings at temperatures ∼150 K, the aggregates as well as the ice matrix are still extremely rigid for large molecules to rotate or translate. However, during the amorphous to crystalline ice phase transition, translational and rotational motions of water molecules occur[30,31] allowing mobility of large molecules leading to the aggregation process of organic impurities. Thus, excimer emission is expected from only those aggregates with their molecular orientation close to the minimum energy orientation seen in crystalline pyrene (that forms excimer) with a pair or pyrene molecules π-stacked,[37−40] whereas the rest of the aggregates undergo either weaker fluorescence or radiationless deactivation through ion-pair formation.[36] Our observations are in full agreement with fluorescence and excimer spectra measured from thin pyrene crystals between 5 and 300 K,[41] where maximum excimer emission is observed at higher temperatures (>70 K) and at >140 K little or no

dx.doi.org/10.1021/jp509513s | J. Phys. Chem. A 2015, 119, 2607−2613

monomer fluorescence is detected. Other studies on pyrene-doped polymer films show similar absorption and emission patterns: from monomer at lower concentration to aggregate at higher concentrations of pyrene in the film.[42] On the basis of this comparison, we propose that upon annealing pyrene-doped water-ice, along with amorphous to crystalline ice transition, pyrene aggregation occurs.

The ice film thickness (Figures 2–4) was estimated to be 350 nm on the basis of the integrated IR absorbance between 2800 and 3700 cm^{-1} and laser interference studies we conducted using HeNe laser. We made thicker ice with the same concentration of pyrene, but 6 times longer deposition duration resulting in ~2000 nm films. These films needed approximately 6 times more time to convert to crystalline ices. However, during the warm-up there were sufficient statistical "excimer" orientations in the ice such that we could easily follow monomer and excimer emissions by exciting into the monomer (332 nm) or aggregate (343 nm) absorptions. These results are summarized in Figure 5. We also want to emphasize that the

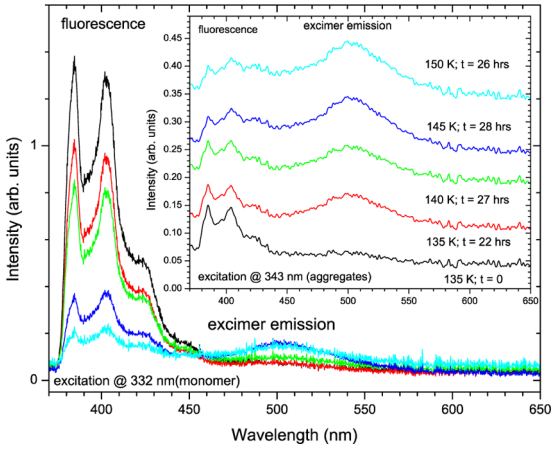

Figure 5. Fluorescence and excimer emission from a 2 μm thick amorphous ice film containing 0.2% pyrene. Excimer emission can be seen already after annealing the ice at 135 K for 22 h (inset). However, a significant amount of monomer fluorescence is seen at this point, indicating that only part of the ice is crystalline. Subsequent warm-ups to higher temperature increase the excimer emission, correlating with a decrease in monomer emission.

aggregation upon annealing ice is a thermodynamically equilibrated energy minimum orientation (similar to nanocrystals) that is not observed when the concentration of pyrene is increased in the amorphous ice or when pyrene is directly deposited without water at low-temperatures, which results in kinetically controlled disordered amorphous phase both with or without the presence of water.[43]

We conducted quantitative kinetics at 135 K on another thin ice film (350 nm), similar to the one used for data shown in Figures 2–4. These results are summarized in Figure 6. After deposition at 30 K, the ice was warmed to 135 K at a rate of 5 K/min. Once the temperature is reached, the ice was kept at that temperature and spectra were recorded periodically. Similar to the UV and IR spectra shown in Figures 2–4, we see that ice infrared absorption gradually transforms from amorphous to crystalline absorption features, correlating well with the pyrene UV absorption features transforming from isolated monomer to aggregates. Each of the intermediate UV spectra could be simulated as a linear combination of the beginning (135 K, t = 0) and end (135 K, t = 23 h) spectra.

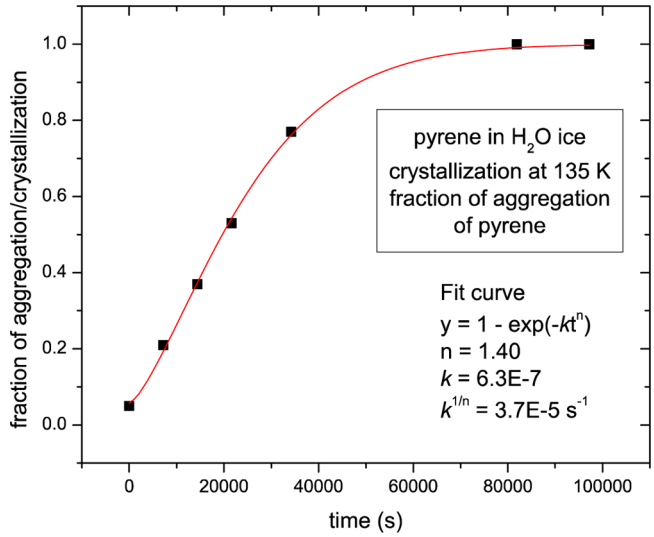

Figure 6. Time vs fraction of crystallization plot for pyrene in amorphous ice kept at 135 K. The fit function is also shown in the plot, which yields a power of 1.4 for time and a rate constant of 3.7 × 10^{-5} s^{-1} for crystallization at 135 K.

From these simulations we derived the fraction of aggregation (x), which we assume is directly correlated to the fraction of crystallization. As shown in Figure 6, we derived an exponent of 1.4 for the time and a rate coefficient ($k^{1/n}$) of 3.7 × 10^{-5} s^{-1} for crystallization at 135 K. These values are in agreement with and extend very well the ice crystallization kinetics measured by Hage et al.[44] that has been compiled by Jenniskens and Blake.[30] For $1/T$ = 0.0074 (135 K), extrapolation of the Hage et al. curve yields a value of ~(2–3) × 10^{-5} s^{-1}, whereas the slower rate (II) of Jenniskens and Blake is ~6 × 10^{-5} s^{-1}. Although the thickness of ice film and the substrate material may play an important role in the crystallization kinetics on a coldfinger that is heated to retain a particular temperature, the interrogation methods may also contribute toward the crystallization process. For example, weak infrared, UV, and laser radiation is used in our studies, whereas Hage et al. used infrared only. In contrast, electron diffraction studies by Jenniskens and Blake used ~50 nm thin films (in contrast to 350–2000 nm in our studies) and high-energy electrons that may facilitate the nucleation process (need not be damage, which the authors clearly state that damage bias is avoided by moving the sample each time to a new position for taking the diffraction pattern). In spite of all these differences, the rates of crystallization obtained in all the three studies tend to agree well for the slower crystallization process.

The results presented here are for pyrene (one of the PAH molecules), which is well-known to show excimer emission. However, due to the fact that the majority of PAHs, at least the medium-sized (~10–40 carbons), have similar polarizabilities and dipole moments, making their interaction with water-ice purely dispersive and van der Waals dominated. We expect, therefore, the medium-size PAHs to behave similarly to pyrene. Large-size PAHs may not be as mobile as the medium-size PAHs, but they can be treated as particles, which may be similar to silicate grains. We also expect a similar aggregation process for aliphatic hydrocarbons, whether saturated or unsaturated. In fact, it has been shown that even methanol undergoes phase separation from a water/methanol amorphous ice mixtures.[45] These authors show that a small portion of methanol (5%) is

dx.doi.org/10.1021/jp509513s | J. Phys. Chem. A 2015, 119, 2607–2613

accommodated into clathrate−hydrate formation during warm-up of amorphous water-ice containing methanol and the rest underwent phase separation during ice crystallization. Thus, we expect our results presented here to be generally applicable to a wide variety of hydrocarbons, the extent of their aggregation dictated by their ability to form clathrates and hydrogen-bonded complexes with the host matrix (water).

IMPLICATIONS

Comets. If the cometary nucleus is made of amorphous ice grains retaining the interstellar ice grain composition, then their surface composition can be explained on the basis of expulsion of material during ice crystallization. A comet goes through significant thermal and radiation variation, from over 300 K to 120 K for a short period Jupiter family comet and a large amount of solar photons and solar wind as a comet approaches its perihelion. Thus, the surface of a comet that started its journey for the first time toward the Sun should get warmed up above 200 K (similar to the comet 67P/Churyumov-Gerasimenko being approached by the Rosetta spacecraft: further details at http://rosetta.esa.int/) even at 3 AU distance, at which point the majority of surface amorphous ice would have crystallized, expelling a significant amount of volatiles as well as nonvolatile refractory organics (cometary organic dust that eventually forms the surface crust of a comet) such as the PAHs studied in this work, mostly in highly oxidized form due to photochemistry.[46,47] These nonvolatile refractory organics would form the surface crust of a comet, mixing with the silicate grains, even as a freshly scattered KBO object becomes a comet during its first journey toward the Sun. Due to the fact that the comets are highly porous,[48] interiors as deep as a meter or two could be well protected from the surface heating during a comet's journey at closer distances to Sun. During each orbit it is expected that the organic/silicate mixed crust of a comet increases in thickness and subsurface amorphous ice grains turn crystalline expelling both volatiles and nonvolatile organics. Crystalline water-ice itself sublimes at higher temperatures when approaching perihelion (closer to the Sun). During this highly active phase of cometary outgassing, some of the surface organic refractory crust is also expected to sublime off.

Icy Moons. Icy moons in our solar system are mostly in the outer solar system at 5 AU and beyond. However, the temperatures at which these moons exist are above 100 K, making their surface and interior water-ice mostly crystalline on the basis of the estimates using laboratory data.[29] This implies that these icy moons with crystalline ices would have expelled the majority of their impurities, making their surfaces mostly crystalline water-ice with a small amount (5−10%) of impurities trapped within the ice crystals or in the defect sites of the crystals, compared to up to 50% or more impurity loading in amorphous ices. This is in agreement with the observations of O_2, H_2O_2, and CO_2 on Europa and Ganymede,[49−54] dominant sulfate features on the radiation bombarded trailing side of Europa, and similar geology on Iapetus with mostly organic/mineral dominated trailing hemisphere that is subjected to micrometeorite bombardment. Upon radiation- or impact-induced heating, crystalline water-ice would sublime, leaving nonvolatile refractory materials whether organics or salts that are already expelled from the crystal lattice of crystalline ice.

Atmospheric and Earth Surface Ice Chemistry. Similar to our results here, where amorphous ices transform into crystalline ices expelling impurity organics, on Earth, liquid water freezes to crystalline ice with salt and other impurities. Though our work comes from a different temperature direction, the end product (crystalline ice) is the same. On Earth, ices are crystalline and they occur at higher temperatures than what we so far measured (~160 K). Crystalline ice persists at much higher temperatures and higher pressures (e.g., 273 K, 1 bar at Earth's surface), and we expect expulsion/aggregation of organics to occur in parallel to the ice nucleation process in Earth's atmosphere. Though our studies are not conducted at these temperatures, the physical processes of aggregation should be applicable to higher temperature and pressure conditions. We expect only a few percent of organics (such as PAHs produced from combustion processes on Earth and in Air traffic; volatile organic compounds, VOCs) to be incorporated into the ice grains as clathrate−hydrates, the rest forming either the core or surface mantle of these ice grains. High-altitude clouds such as the polar stratospheric clouds (PSCs), polar mesospheric clouds (PMCs), and cirrus clouds all consist of ice grains.[55−57] Ice packs on high-altitude mountains and the ice sheets in the polar regions also contain crystalline ice in equilibrium with liquid water that can accommodate larger amounts of impurities. With increasing amounts of organic pollutants in our atmosphere, these organics make their way to polar ices as well as into the upper atmosphere.[58,59] On the basis of our experimental results, we expect organics to be trapped not in the ice crystal lattice, but in the ice grain boundaries, which would be the active site of chemical processes.

CONCLUSIONS

Expulsion of impurity molecules from crystalline ices is an important phenomenon that has implications to Earth's surface and atmospheric ices, Solar System ices, and interstellar ice grains. This phenomenon could also play a critical role in cryobiology and survival of organisms in cold and icy environments. Though amorphous ices are known to accommodate a large fraction of impurities by trapping them in their structureless and porous matrix, we have shown that when these amorphous ices undergo crystallization, these impurities are expelled from the crystal lattice, leading to the formation of aggregates. Our studies also provide a qualitative mechanism for the formation of cometary organic crust; aggregation of organics should also occur on icy bodies in our solar system such as Europa, Ganymede, and Enceladus, where crystalline ice dominates. Quantitative data derived at 135 K for the rate of crystallization of amorphous ices is in agreement with the literature data, opening an easy method to study the crystallization process of amorphous ices at a wide temperature range using diluted PAH molecules as probes. In agreement with literature reports on substituted pyrene aggregates, we have shown here that UV absorption spectra of pyrene could be very sensitive probes for monomer vs aggregate formation in condensed media. Pyrene is an excellent model system for such studies, and it has been shown over half a century ago by Förster and Kasper that its emission properties change on the basis of its aggregation.[35]

AUTHOR INFORMATION

Corresponding Author

*M. S. Gudipati. Tel: +1-818-354-2637. E-mail: murthy.gudipati@jpl.nasa.gov.

Present Address

[‡]Finnish Academy of Science Post Doctoral Fellow at the Jet Propulsion Laboratory; Arthur Amos Noyes Laboratory of Chemical Physics, California Institute of Technology, MC 127-72 1200 East California Boulevard, Pasadena, CA 91125, USA.

Notes

The authors declare no competing financial interest.

[§]Also a senior research scientist at IPST, University of Maryland, College Park, MD 20742, United States

■ ACKNOWLEDGMENTS

This research was enabled through partial funding from the following NASA programs: Planetary Atmospheres, Cassini Data Analysis Programs, Spitzer Science Center, and Astrobiology Institute Node Early Habitable Environments (NASA Ames). JPL's DRDF and R&TD funding for infrastructure of the "ice spectroscopy laboratory" is also gratefully acknowledged. This research was carried out at the Jet Propulsion Laboratory, California Institute of Technology, under a contract with the National Aeronautics and Space Administration.

■ REFERENCES

(1) van Dishoeck, E. F.; Herbst, E.; Neufeld, D. A. Interstellar Water Chemistry: From Laboratory to Observations. *Chem. Rev.* **2013**, *113*, 9043−9085.

(2) Oberg, K. I.; Boogert, A. C. A.; Pontoppidan, K. M.; van den Broek, S.; van Dishoeck, E. F.; Bottinelli, S.; Blake, G. A.; Evans, N. J. The Spitzer Ice Legacy: Ice Evolution from Cores to Protostars. *Astrophys. J.* **2011**, *740*, 109.

(3) Brown, M. E. The Compositions of Kuiper Belt Objects. *Annu. Rev. Earth Planet. Sci.* **2012**, *40*, 467−494.

(4) Jewitt, D. C.; Luu, J. Crystalline Water Ice on the Kuiper Belt Object (50000) Quaoar. *Nature* **2004**, *432*, 731−733.

(5) Luu, J. X.; Jewitt, D. C. Kuiper Belt Objects: Relics from the Accretion Disk of the Sun. *Annu. Rev. Aston. Astrophys.* **2002**, *40*, 63−101.

(6) Bar-Nun, A.; Herman, G.; Laufer, D. Trapping and Release of Gases by Water Ice and Implications for Icy Bodies. *Icarus* **1985**, *63*, 317−332.

(7) Kossacki, K. J.; Szutowicz, S. Crystallization of Ice in Comet 17p/Holmes: Probably Not Responsible for the Explosive 2007 Megaburst. *Icarus* **2010**, *207*, 320−340.

(8) Marboeuf, U.; Petit, J. M.; Mousis, O. Can Collisional Activity Produce a Crystallization of Edgeworth-Kuiper Belt Comets? *Mon. Not. R. Astron. Soc.* **2009**, *397*, L74−L78.

(9) Gonzalez, M.; Gutierrez, P. J.; Lara, L. M.; Rodrigo, R. Evolution of the Crystallization Front in Cometary Models. *Astron. Astrophys.* **2008**, *486*, 331−340.

(10) Prialnik, D.; Barnun, A. Crystallization of Amorphous Ice as the Cause of Comet P-Halley Outburst at 14-Au. *Astron. Astrophys.* **1992**, *258*, L9−L12.

(11) Martins, Z.; Price, M. C.; Goldman, N.; Sephton, M. A.; Burchell, M. J. Shock Synthesis of Amino Acids from Impacting Cometary and Icy Planet Surface Analogues. *Nat. Geosci.* **2013**, *6*, 1045−1049.

(12) Goldman, N.; Reed, E. J.; Fried, L. E.; Kuo, I. F. W.; Maiti, A. Synthesis of Glycine-Containing Complexes in Impacts of Comets on Early Earth. *Nat. Chem.* **2010**, *2*, 949−954.

(13) Oberbeck, V. R.; Aggarwal, H. Comet Impacts and Chemical Evolution on the Bombarded Earth. *Origins Life Evol. Biospheres* **1992**, *21*, 317−338.

(14) McNaughton, N. J.; Pillinger, C. T. Comets and the Origin of Life. *Nature* **1980**, *288*, 540−540.

(15) Irvine, W. M.; Leschine, S. B.; Schloerb, F. P. Thermal History, Chemical-Composition and Relationship of Comets to the Origin of Life. *Nature* **1980**, *283*, 748−749.

(16) Bottke, W. F.; Vokrouhlicky, D.; Minton, D.; Nesvorny, D.; Morbidelli, A.; Brasser, R.; Simonson, B.; Levison, H. F. An Archaean Heavy Bombardment from a Destabilized Extension of the Asteroid Belt. *Nature* **2012**, *485*, 78−81.

(17) Stotler, R. L.; Frape, S. K.; Ruskeeniemi, T.; Ahonen, L.; Onstott, T. C.; Hobbs, M. Y. Hydrogeochemistry of Groundwaters in and Below the Base of Thick Permafrost at Lupin, Nunavut, Canada. *J. Hydrol.* **2009**, *373*, 80−95.

(18) Mtombeni, T.; Maree, J. P.; Zvinowanda, C. M.; Asante, J. K. O.; Oosthuizen, F. S.; Louw, W. J. Evaluation of the Performance of a New Freeze Desalination Technology. *Int. J. Environ. Sci. Technol.* **2013**, *10*, 545−550.

(19) Mandri, Y.; Rich, A.; Mangin, D.; Abderafi, S.; Bebon, C.; Semlali, N.; Klein, J. P.; Bounahmidi, T.; Bouhaouss, A. Parametric Study of the Sweating Step in the Seawater Desalination Process by Indirect Freezing. *Desalination* **2011**, *269*, 142−147.

(20) Rich, A.; Mandri, Y.; Bendaoud, N.; Mangin, D.; Abderafi, S.; Bebon, C.; Semlali, N.; Klein, J. P.; Bounahmidi, T.; Bouhaouss, A.; Vessler, S. Freezing Desalination of Sea Water in a Static Layer Crystallizer. *Desalin. Water Treat.* **2010**, *13*, 120−127.

(21) Roser, J. E.; Allamandola, L. J. Infrared Spectroscopy of Naphthalene Aggregation and Cluster Formation in Argon Matrices. *Astrophys. J.* **2010**, *722*, 1932−1938.

(22) Szczepanski, J.; Fuller, J.; Ekern, S.; Vala, M. Electronic Absorption and Resonance Raman Spectra of Large Linear Carbon Clusters Isolated in Solid Argon. *Spectrochim. Acta, Part A* **2001**, *57*, 775−786.

(23) Markus, R.; Moutard, P.; Chergui, M.; Schwentner, N. Spectroscopy and Photochemistry of Au Aggregates in Rare-Gas Matrices. *J. Lumin.* **1988**, *40*−*1*, 260−261.

(24) Mitchell, S. A.; Ozin, G. A. Silver Clusters in Rare-Gas Matrices - Thermal and Photochemical Silver Atom Aggregation Reactions. *J. Phys. Chem.* **1984**, *88*, 1425−1436.

(25) Barnett, I. L.; Lignell, A.; Gudipati, M. S. Survival Depth of Organics in Ices under Low-Energy Electron Radiation ($\lesssim$ 2 keV). *Astrophys. J.* **2012**, *747*, 13.

(26) Hardegree-Ullman, E. E.; Gudipati, M. S.; Boogert, A. C. A.; Lignell, H.; Allamandola, L. J.; Stapelfeldt, K. R.; Werner, M. Laboratory Determination of the Infrared Band Strengths of Pyrene Frozen in Water Ice: Implications for the Composition of Interstellar Ices. *Astrophys. J.* **2014**, *784*, 172.

(27) Herbst, E. Three Milieux for Interstellar Chemistry: Gas, Dust, and Ice. *Phys. Chem. Chem. Phys.* **2014**, *16*, 3344−3359.

(28) Hama, T.; Watanabe, N. Surface Processes on Interstellar Amorphous Solid Water: Adsorption, Diffusion, Tunneling Reactions, and Nuclear-Spin Conversion. *Chem. Rev.* **2013**, *113*, 8783−8839.

(29) Mastrapa, R. E.; Grundy, W.; Gudipati, M. Amorphous and Crystalline H2O-Ice. In *The Science of Solar System Ices*; Gudipati, M. S., Castillo-Rogez, J., Eds.; Springer: New York, 2013; Vol. *356*, pp 371−408.

(30) Jenniskens, P.; Blake, D. F. Crystallization of Amorphous Water Ice in the Solar System. *Astrophys. J.* **1996**, *473*, 1104−1113.

(31) Jenniskens, P.; Blake, D. F. Structural Transitions in Amorphous Water Ice and Astrophysical Implications. *Science* **1994**, *265*, 753−756.

(32) Grundy, W. M.; Schmitt, B. The Temperature-Dependent near-Infrared Absorption Spectrum of Hexagonal H2O Ice. *J. Geophys. Res.: Planets* **1998**, *103*, 25809−25822.

(33) Gudipati, M. S. Matrix-Isolation in Cryogenic Water-Ices: Facile Generation, Storage, and Optical Spectroscopy of Aromatic Radical Cations. *J. Phys. Chem. A* **2004**, *108*, 4412−4419.

(34) Siu, H.; Duhamel, J. Molar Absorption Coefficient of Pyrene Aggregates in Water. *J. Phys. Chem. B* **2008**, *112*, 15301−15312.

(35) Förster, T.; Kasper, K. Ein Konzentrationsumschlag Der Fluoreszenz Des Pyrens. *Z. Elektrochem., Ber. Bunsen-Ges. Phys. Chem.* **1955**, *59*, 976−980.

(36) Ito, F.; Kakiuchi, T.; Sakano, T.; Nagamura, T. Fluorescence Properties of Pyrene Derivative Aggregates Formed in Polymer Matrix Depending on Concentration. *Phys. Chem. Chem. Phys.* **2010**, *12*, 10923−10927.
(37) Nakamura, M.; Fukuda, M.; Takada, T.; Yamana, K. Highly Ordered Pyrene Pi-Stacks on an Rna Duplex Display Static Excimer Fluorescence. *Org. Biomol. Chem.* **2012**, *10*, 9620−9626.
(38) Nakagawa, K.; Numata, Y.; Ishino, H.; Tanaka, D.; Kobayashi, T.; Tokunaga, E. Excimer Luminescence from Nonresonantly Excited Pyrene and Perylene Molecules in Solution. *J. Phys. Chem. A* **2013**, *117*, 11449−11455.
(39) Camerman, A.; Trotter, J. Crystal Molecular Structure of Pyrene. *Acta Crystallogr.* **1965**, *18*, 636−643.
(40) Knight, K. S.; Shankland, K.; David, W. I. F.; Shankland, N.; Love, S. W. The Crystal Structure of Perdeuterated Pyrene II at 4.2 K. *Chem. Phys. Lett.* **1996**, *258*, 490−494.
(41) Seyfang, R.; Port, H.; Fischer, P.; Wolf, H. C. Picosecond Study on Excimer Formation in Pyrene Crystals 0.3. Complete Analysis of the High-Temperature Phase between 5 and 300-K. *J. Lumin.* **1992**, *51*, 197−208.
(42) Pujari, S. R.; Kambale, M. D.; Bhosale, P. N.; Rao, P. M. R.; Patil, S. R. Optical Properties of Pyrene Doped Polymer Thin Films. *Mater. Res. Bull.* **2002**, *37*, 1641−1649.
(43) Cuylle, S. H.; Allamandola, L. J.; Linnartz, H., Photochemistry of PAHs in Cosmic Water Ice the Effect of Concentration on UV-Vis Spectroscopy and Ionization Efficiency. *Astron. Astrophys.* **2014**, *562*.
(44) Hage, W.; Hallbrucker, A.; Mayer, E.; Johari, G. P. Crystallization Kinetics of Water Below 150 K. *J. Chem. Phys.* **1994**, *100*, 2743−2747.
(45) Blake, D.; Allamandola, L.; Sandford, S.; Hudgins, D.; Freund, F. Clathrate Hydrate Formation in Amorphous Cometary Ice Analogs Invacuo. *Science* **1991**, *254*, 548−551.
(46) Gudipati, M. S.; Cooper, P. D., Chemistry in Water Ices: From Fundamentals to Planetary Applications. In *The Science of Solar System Ices*; Gudipati, M. S., Castillo-Rogez, J., Eds.; Springer: New York, 2013; Vol. 356, pp 503−526.
(47) Gudipati, M. S.; Yang, R. In-Situ Probing of Radiation-Induced Processing of Organics in Astrophysical Ice Analogs: Novel Laser Desorption Laser Ionization Time-of-Flight Mass Spectroscopic Studies. *Astrophys. J. Lett.* **2012**, *756*, L24.
(48) Thomas, P. C.; A'Hearn, M. F.; Veverka, J.; Belton, M. J. S.; Kissel, J.; Klaasen, K. P.; McFadden, L. A.; Melosh, H. J.; Schultz, P. H.; Besse, S.; Carcich, B. T.; Farnham, T. L.; Groussin, O.; Hermalyn, B.; Li, J. Y.; Lindler, D. J.; Lisse, C. M.; Meech, K.; Richardson, J. E. Shape, Density, and Geology of the Nucleus of Comet 103p/Hartley 2. *Icarus* **2013**, *222*, 550−558.
(49) Vidal, R. A.; Bahr, D.; Baragiola, R. A.; Peters, M. Oxygen on Ganymede: Laboratory Studies. *Science* **1997**, *276*, 1839−1842.
(50) Spencer, J. R.; Calvin, W. M.; Person, M. J. Charge-Coupled-Device Spectra of the Galilean Satellites - Molecular-Oxygen on Ganymede. *J. Geophys. Res.: Planets* **1995**, *100*, 19049−19056.
(51) Hansen, G. B.; McCord, T. B. Widespread CO2 and Other Non-Ice Compounds on the Anti-Jovian and Trailing Sides of Europa from Galileo/Nims Observations. *Geophys. Res. Lett.* **2008**, *35*, L01202.
(52) Spencer, J. R.; Grundy, W. M.; Dumas, C.; Carlson, R. W.; McCord, T. B.; Hansen, G. B.; Terrile, R. J. The Nature of Europa's Dark Non-Ice Surface Material: Spatially-Resolved High Spectral Resolution Spectroscopy from the Keck Telescope. *Icarus* **2006**, *182*, 202−210.
(53) Dalton, J. B. Linear Mixture Modeling of Europa's Non-Ice Material Based on Cryogenic Laboratory Spectroscopy. *Geophys. Res. Lett.* **2007**, *34*, L21205.
(54) Hand, K. P.; Brown, M. E., Keck Ii Observations of Hemispherical Differences in H2O2 on Europa. *Astrophys. J. Lett.* **2013**, *766*.
(55) Rong, P. P.; Russell, J. M.; Randall, C. E.; Bailey, S. M.; Lambert, A. Northern Pmc Brightness Zonal Variability and Its Correlation with Temperature and Water Vapor. *J. Geophys. Res.: Atmos.* **2014**, *119*, 2390−2408.
(56) Engel, I.; Luo, B. P.; Pitts, M. C.; Poole, L. R.; Hoyle, C. R.; Grooss, J. U.; Dornbrack, A.; Peter, T. Heterogeneous Formation of Polar Stratospheric Clouds - Part 2: Nucleation of Ice on Synoptic Scales. *Atmos. Chem. Phys.* **2013**, *13*, 10769−10785.
(57) Shibata, T.; Vomel, H.; Hamdi, S.; Kaloka, S.; Hasebe, F.; Fujiwara, M.; Shiotani, M. Tropical Cirrus Clouds near Cold Point Tropopause under Ice Supersaturated Conditions Observed by Lidar and Balloon-Borne Cryogenic Frost Point Hygrometer. *J. Geophys. Res.: Atmos.* **2007**, *112*, D03210.
(58) Anastasio, C.; Hoffmann, M.; Klán, P.; Sodeau, J., Photochemistry in Terrestrial Ices. In *The Science of Solar System Ices*; Gudipati, M. S., Castillo-Rogez, J., Eds.; Springer: New York, 2013; Vol. 356, pp 583−644.
(59) Hellebust, S.; O'Riordan, B.; Sodeau, J. Cirrus Cloud Mimics in the Laboratory: An Infrared Spectroscopy Study of Thin Films of Mixed Ice of Water with Organic Acids and Ammonia. *J. Chem. Phys.* **2007**, *126*, 084702.